Numerical Investigation of Bouncing Vibrations of an Air Bearing Slider in Near or Partial Contact

Du Chen and David B. Bogy

Computer Mechanics Laboratory

Dept. of Mechanical Engineering

University of California

Berkeley, CA 94720

Abstract

The bouncing vibration of an air bearing slider in near or partial contact with the disk is numerically analyzed using three different nonlinear slider dynamic models. The near or partial contact slider is designed for the future areal recording density in hard disk drives of 1 Tbit/in^2 or even higher. In these three slider dynamic models, the air bearing with contact is modeled either using the generalized Reynolds equation modified with the Fukui-Kaneko slip correction and a new second order slip correction for the contact situation, or using nonlinear springs to represent the air bearing. The contact and adhesion between the slider and the disk are considered either through an elastic contact model and an improved intermolecular adhesion model, respectively, or using an Ono-Yamane [1] multi-asperity contact and adhesion model. The contact friction is calculated through Coulomb's law. The simulation results from all models show that the slider's bouncing vibration occurs as a forced vibration caused by the micro-waviness and

roughness. The disk surface micro-waviness and roughness, which move into the head disk interface (HDI) as the disk rotates, excite the bouncing vibration of the partial contact slider. The contact, adhesion and friction between the slider and the disk do not directly cause a bouncing vibration in the absence of disk micro-waviness or roughness.

1. Introduction

Reducing the flying height (FH) of sliders is a requirement for achieving higher recording densities in hard disk drives. The Wallace spacing loss equation indicates that the magnetic signal decreases exponentially as the distance increases between the magnetic layer and the read/write transducer. The maximum magnetic signal can be obtained at a spacing of zero, but this would require direct contact with the magnetic layer and is therefore impractical with current magnetic media.

There are several contact HDI interface designs under consideration for the planned magnetic recording density of 1 Tbit/in^2 or even higher in Hard Disk Drives (HDD): "wear in", "proximity", and "full contact". It is expected that all of these technologies, except possibly the last one, will rely on an air bearing to support most of the suspension load, while the trailing pad of the slider is in contact with the disk at the beginning, frequently or continuously. In this sense the HDI has at least partial contact.

In this paper three different nonlinear slider dynamic models are used to numerically analyze the vertical bouncing vibration of an air bearing slider in the near or partial contact region. Numerical simulations of the slider's dynamics show that the slider's bouncing vibration is a forced vibration caused by the micro-waviness and roughness. The disk surface micro-waviness and roughness, which move into the head disk interface (HDI) as the disk rotates, excite the bouncing vibration of the partial contact slider. The

contact, adhesion and friction between the slider and the disk do not directly cause a bouncing vibration in the absence of disk micro-waviness or roughness.

2. Dynamics, ahesion and contact models

The generalized time-dependent Reynolds equation is used to model the air bearing between the partial contact slider and the disk. The Reynolds equation is modified using the Fukui-Kaneko (FK) slip correction [2] to account for the rarefaction of the ultra thin air film within the slider-disk spacing. As indicated by Wu and Bogy [3], the FK correction produces an unbounded contact pressure singularity at contact. They proposed a new second order slip model that avoids the pressure singularity, which predicts results not far from the FK correction when the modified inverse Knudsen number is not too large. For the contact region in an air bearing, Huang and Bogy [4] adopted in their Monte Carlo method a no-fly-zone condition, which assumes that air molecules can not enter a gap smaller than themselves. Here we combine the FK model and the new second order slip model. When the air film thickness is larger than 0.3 nm, which is approximately the diameter of an oxygen or nitrogen atom, the FK model is used; when it is less than 0.3 nm, the new second order slip model is used to avoid the pressure singularity.

A simple alternative air bearing model uses non-linear springs to represent the air bearing [1]. The air bearing of the entire air bearing surface is modeled with a front lumped nonlinear spring, a front linear dashpot, a rear lumped nonlinear spring and a rear linear dashpot. The springs and dashpots are located at the front or rear air bearing pressure center. The spring stiffness values are chosen to match otherwise calculated or

experimentally measured air bearing frequencies. And the damping coefficients are determined by preset damping ratios.

The impact between the partial contact slider and the disk is quasi-static and therefore can be modeled using an elastic contact model based on the static influence coefficient matrix, as described in [5]. We use this model instead of asperity contact models, such as the CEB model [6], because those models assume that the bulk deformation and interactions between asperities are negligible. For a partial contact HDI, the flying height at some parts of the air bearing surface (ABS) might be negative, which means that the distance between those parts of the slider and the undeformed disk surface is less than zero. Under this condition, the bulk deformation and interactions between asperities may not be negligible. However, one simplification in those models is retained here. The contact between two rough surfaces can be approximated as the contact between a rigid smooth surface and an equivalent elastic rough surface [7]. So in the simulations we consider the equivalent contact between smooth slider pads and a rough disk surface.

Because of the bulk deformation, asperity adhesion models and asperity-based friction models are also not suitable for the dynamic simulation of the partial contact HDI. Here adhesion is calculated through the improved intermolecular force model [8], which does not predict an infinite repulsion when the slider and disk are in contact. The effect of the lubricant is modeled through the value of the surface energy difference before and after contact. Coulomb's law is used for the friction between the slider and disk.

Another slider-disk contact and adhesion model, developed by Ono and Yamane [1], is also used here for comparison. It is a complicated multi-asperity contact and adhesion

model, which considers the bulk deformation of the contact interface and assumes that the lubricant meniscus is the only source of adhesion between the slider and disk. This model gives a stochastically averaged contact and adhesion force and the effect of asperities, which model the equivalent rough disk surface, on the air bearing is not considered. In this model the contact and adhesion forces between a slider and a disk are functions of the spacing between the contact pad and the disk, given the statistical characteristics of the roughness on the disk surface (including the radius of curvature of asperities, the asperity density and the standard deviation of asperity heights), the contact pad area and the surface energy of the lubricant. With the assumption that the contact area does not change at any interference depth, the slider-disk contact characteristics can be simply described using the maximum value of adhesion force, the bulk contact stiffness, the initial real contact force at the beginning of contact and the touch-down and take-off flying heights [1].

3. Three slider dynamic models

Two slider dynamic models are obtained by implementing the two sets of contact and adhesion models discussed above into the CML slider dynamic air bearing program. The ABS is discretized into small grids, which are approximately parallel to the disk surface with various flying heights. The modified Reynolds equation is then discretized using Patankar's control volume method, and the final discretization equations are solved using the alternating direction line sweep method combined with the full multi-grid algorithm. The dynamic program uses the Newmark Beta method to solve the slider dynamics equations.

The third slider dynamic model analyzed in this report is the two-degree-of-freedom (2-DOF) slider model developed by Ono and Yamane [1]. It includes the nonlinear air bearing spring model and the simplified multi-asperity contact and adhesion model. The 4th order Runger-Kutta method is used to solve the slider's equations of motion, as was done in [1].

4. Slider Dynamic Simulation and results

Dynamic simulations using the CML air bearing model, the elastic contact model and the modified intermolecular force model

Using the first model described above we analyze the vertical bouncing vibration of a partial contact HDI. We employ micro-trailing pad sliders in the simulations. As was found in [9], a slider in the contact regime with a smaller trailing pad may incur smaller short range attractive forces between the slider and disk as well as a reduced contact force. This helps to decrease the slider's tendency to crash in the partial contact process. The ABS design of the slider is shown in Fig. 1.

Here three different disk surfaces are used in the simulation. The first is an ideally flat disk surface, i.e. the RMS of the surface roughness is zero; the second is a "rough" disk surface with RMS roughness equal to 0.2 nm; the third is the same rough disk surface, but the disk micro-waviness and roughness within the HDI remains stationary. The third case is not practical, since the disk surface profile within the HDI keeps changing with the disk rotation. But we use this case to analyze the effect of dynamic roughness on the partial contact HDI.

Fig. 2 shows the time histories of the minimum spacing between the slider and the mean plane of the disk surface, the pitch, the roll, and the corresponding power spectra of

the minimum spacing for these three cases. We can see that in case I and case III the initial response of the slider to the loading process is quickly damped out and the slider achieves a continuous contact steady state. However, in case II the slider keeps bouncing on the disk surface and the bouncing vibrations can not be damped. The frequency spectra of the minimum spacing in case I and case III are similar, while the frequency spectrum in case II is different and it has a series of peaks around 800 kHz. These higher frequency components are evidently associated with the slider-disk contact. The micro-waviness and roughness on the disk surface, which move into the HDI as the disk rotates, excite these high frequency components, and they cause the slider's continuous vertical bouncing vibration.

Dynamic simulations using the CML air bearing model and the multi-asperity contact and meniscus adhesion model of Ono and Yamane

Ono and Yamane [1] successfully implemented their multi-asperity contact and adhesion model in their 2-DOF slider dynamic model to study the unsteady bouncing vibration of low flying height sliders on a disk surface without micro-waviness or roughness. They reached a conclusion that the bouncing vibration can also be a self-excited vibration caused by the adhesion and friction forces in the absence of moving disk micro-waviness or roughness. This is different from the conclusion presented above.

To analyze this self-excited vibration, Ono and Yamane's contact and adhesion model [1] is incorporated in the CML slider dynamic model in place of the elastic contact and improved intermolecular force models used above. First, in order to avoid the difficulties in applying this contact and adhesion model to the 3-DOF slider model in the CML air bearing program, we reduce the CML slider model to a 2-DOF one by inputting a huge

suspension roll stiffness so that the motion in the roll direction is negligible. Second, the simplified contact characteristic model is used instead of the full multi-asperity contact and adhesion model. The contact area is assumed to be constant and the statistical characteristics of the equivalent disk surface are the same as those used by Ono and Yamane. The separation between the contact pad and the mean disk surface is assumed to be equal to the minimum spacing between the slider and the mean disk surface. Here we fix the bulk contact stiffness to be 5.0×10^6 N/m, the initial contact force to be 5.0 mN and the touch-down FH to be 3.0 nm. Values of the minimum adhesion force, the bulk contact stiffness and the takeoff flying height are shown in Table I, where those with an upper asterisk are the default values used in the simulations.

The force hysteresis needs to be considered in implementing Ono and Yamane's model. Fig. 3 shows the relations of the real contact force F_{cr}, adhesion force F_m, contact force F_c (the sum of real contact and adhesion force) versus the separation d between the contact pad and the disk in the simplified model. The arrows on the lines denote the touch-down and take-off processes. In the simulation it is assumed that the slider's initial state is touch-down if the initial separation is less than the take-off FH d_e. Then, the slider's current separation d determines the slider's state at the next time step, if the time step size used in the simulation is small enough. When the separation d is larger than d_e, the slider's state at the next time step is touch-down. When the separation d is less than d_s, the slider's state at the next time step is take-off or touch-down, but it can be set to take-off since the touch-down line and take-off line coincide when d is less than d_s. Then the slider's state at the next time step remains the same as the current state when the separation is between d_s and d_e.

A CML slider design is used in the simulation. The air bearing surface is shown in Fig. 4. It is a pico size slider (1.25 mm× 1.00 mm). The suspension preload is 1.5 gram and the disk RPM is 5400. Its static minimum flying height is approximately 3.2 nm and its pitch angle is approximately 176 μrad on a flat disk surface. This means that the disk may contact the slider if the take-off FH is above 3.2 nm. Figs. 5-8 show the time histories of the slider dynamics with different maximum meniscus force, take-off FH, friction coefficient and initial FH, respectively.

The negative contact force in Fig. 5 shows that the flying slider contacts the disk when the maximum meniscus force is increased to 15 mN. However, the slider's bouncing vibration is damped out even when the slider contacts the disk with a negative total contact force.

Figs. 6-8 indicate the existence of two different steady states. Fig. 6 shows that when the take-off FH is 4 nm, the slider does not contact the disk in the steady state; when the take-off FH is 5.5 nm or 8 nm, the slider contacts the disk in the steady state. Fig. 7 shows that the slider contacts the disk in the steady state when the friction coefficient is increased to 2.0. Fig. 8 shows that different initial FHs may also produce different final steady states. With an initial FH of 3.5 or 10 nm the slider does not contact the disk in the steady state; with an initial FH of 5 nm or 20 nm, the slider contacts the disk in the steady state. All of these indicate that the slider may have two different final steady states. One state is a flying state, i.e. the slider does not contact the disk. The other is a contact state with lower spacing, in which the slider contacts the disk with a negative total contact force. This negative total contact force is compensated by the increased air bearing force due to the lower spacing. The final state is determined by the take-off FH, the friction

coefficient or the initial FH. However, the existence of these two steady states does not mean that the slider will vibrate between two states. Instead the slider's bouncing vibration is damped out quickly. In addition, the effect of the friction coefficient and the take-off FH can be seen from the simulation results. The contact steady state in Fig. 7 has a smaller pitch angle than the contact steady state in Fig. 8. This shows that a large friction coefficient may cause a low pitch angle when the slider contacts the disk. In Fig. 6, the slider doesn't contact the disk until the take-off FH is increased beyond 5.5 nm. It corresponds to an experimental observation that higher take-off FH causes a greater likelihood of slider disk contact.

In conclusion, the simulation results of the CML 2-DOF slider dynamic model, which incorporates Ono and Yamane's simple contact characteristic model for the slider disk contact and adhesion, show that the slider-disk contact, adhesion and friction are not the direct cause of the slider's bouncing vibrations. So this implies that the near or partial contact slider-disk interface is not an adhesion and friction caused self-excited system as shown in [1]. The destabilizing mechanism of friction force shown in [1] might not provide a strong proof. On one hand, the work done by the friction to the air bearing-slider-suspension system is not guaranteed to be always positive. On the other hand, not only the friction force between the slider and the disk but also the contact force does work on the slider. The moment arm of the contact force is much larger than that of the friction force, given that the pitch angle is on the order of μrad. From these two points of view, the friction appears not to be the main cause of the slider's vibration. With the statistically averaged contact and adhesion model, it is even found that the adhesion force actually helps to reduce the bouncing vibrations [10].

Analysis using Ono and Yamane's 2-DOF dynamic model

The 2-DOF slider dynamic model of Ono and Yamane [1], with the simple nonlinear air bearing model and the multi-asperity contact and adhesion model, is re-analyzed here in an attempt to obtain a non-decayed bouncing vibration of a slider in the near or partial contact regime on a disk without micro-waviness, which is shown in Section 3.3 of [1]. Fig. 9 shows this 2-DOF system model. The air bearing is simply represented by two lumped nonlinear springs (stiffness coefficients k_f and k_r) and two linear dashpots (damping coefficients c_f and c_r) located at the front and rear bearing pressure centers, respectively. With z_f and z_g denoting the spacing at the front and rear air bearing pressure center, respectively, the air bearing stiffnesses used in the model are expressed as,

$$k_r = \begin{cases} \dfrac{k_{r0} z_{r0}^2}{z_r^2}, \text{when } z_r > d_1 \\ 0, \quad \text{when } z_r < d_1 \end{cases}; k_f = \begin{cases} \dfrac{k_{f0} z_{f0}^2}{z_f^2}, \text{when } z_f > d_1 \\ 0, \quad \text{when } z_f < d_1 \end{cases} \tag{1}$$

where the subscript *0* denotes the parameters in the static state and d_1 is a preset parameter. And the corresponding damping coefficients are $c_f = 2\xi_f \sqrt{M k_{f0}}$ and $c_r = 2\xi_r \sqrt{M k_{r0}}$. The suspension is represented by a normal linear spring (k) and dashpot ($c = 2\xi\sqrt{Mk}$), an angular spring (k_θ) and dashpot ($c_\theta = 2\xi_\theta \sqrt{J k_\theta}$), static load ($F_0$) and static moment ($M_0$). The simplified contact characteristic model shown in Fig. 3 is used to model the slider-disk adhesion and contact.

For a slider with a static flying height FH at the transducer and a static pitch angle θ_0, the equation of motion of the slider is derived in [1] as,

$$\begin{bmatrix} M & 0 \\ 0 & J \end{bmatrix}\begin{Bmatrix} \ddot{z}g \\ \ddot{\theta} \end{Bmatrix}+\begin{bmatrix} c_{11}\ c_{21} \\ c_{21}\ c_{22} \end{bmatrix}\begin{Bmatrix} \dot{z}_g \\ \dot{\theta} \end{Bmatrix}+\begin{bmatrix} k_{11}\ k_{21} \\ k_{21}\ k_{22} \end{bmatrix}\begin{Bmatrix} z_g \\ \theta \end{Bmatrix} = \begin{Bmatrix} F_c(z_p)+F_0(FH,\theta_0) \\ -\frac{1}{2}b\mu F_{cr}(z_p)+d_hF_c(z_p)+M_0(FH,\theta_0) \end{Bmatrix} \tag{2}$$

where z_g denotes the vertical displacement of the center of mass from the mean roughness plane of the disk and θ denotes the angular displacement in the counter clockwise direction from the horizontal line.

Notice that for the static state,

$$\begin{bmatrix} k_{11}\ k_{21} \\ k_{21}\ k_{22} \end{bmatrix}\begin{Bmatrix} z_{g0} \\ \theta_0 \end{Bmatrix} = \begin{Bmatrix} F_0(FH,\theta_0) \\ M_0(FH,\theta_0) \end{Bmatrix} \quad . \tag{3}$$

Then if we define $z_g^{'} = z_g - z_{g0}$ and $\theta^{'} = \theta - \theta_0$, we can re-write the equations of motion as,

$$\begin{bmatrix} M & 0 \\ 0 & J \end{bmatrix}\begin{Bmatrix} \ddot{z}_g^{'} \\ \ddot{\theta}^{'} \end{Bmatrix}+\begin{bmatrix} c_{11}\ c_{21} \\ c_{21}\ c_{22} \end{bmatrix}\begin{Bmatrix} \dot{z}_g^{'} \\ \dot{\theta}^{'} \end{Bmatrix}+\begin{bmatrix} k_{11}\ k_{21} \\ k_{21}\ k_{22} \end{bmatrix}\begin{Bmatrix} z_g^{'} \\ \theta^{'} \end{Bmatrix} = \begin{Bmatrix} F_c(z_p) \\ -\frac{1}{2}b\mu F_{cr}(z_p)+d_hF_c(z_p) \end{Bmatrix} \tag{4}$$

The total energy of the air bearing, slider and suspension system, without considering the elastic contact energy, can be expressed as,

$$E = \frac{1}{2}m\dot{z}_p^2+\frac{1}{2}m\dot{\theta}^2+\frac{1}{2}k(z_g-z_{g0})^2+k_{f0}z_{f0}^2[\frac{z_{f0}}{z_f}-\ln(\frac{z_{f0}}{z_f})-1]+k_{r0}z_{r0}^2[\frac{z_{r0}}{z_r}-\ln(\frac{z_{r0}}{z_r})-1] \tag{5}$$

The same parameter values as used in section 3.3 of [1], which are shown in Table II, are used in the simulation here. The parameter d_1 used in the air bearing model is not discussed in [1]. With the no-fly-zone condition, d_1 can be set to 0.3 nm; or d_1 is set to be equal to d_s [11], which means that the air bearing is lost when the separation is less than the touch-down flying height. We use both of these values in the following simulations.

The 4th order Runger-Kutta method is used to solve the equations of motion as in [1]. If d_1 = 0.3 nm is set, the time history of the slider dynamics of a 7 nm slider with an initial condition of FH = 250 nm and θ = 0 μrad is shown in Fig. 10 (a). It is obvious that the slider's vibration is damped quickly and the slider achieves a steady state, which is the same as its static state. If $d_1 = d_s$, the time history of the slider's dynamics with the same initial conditions is shown in Fig. 10 (b). It is seen that the slider's dynamics doesn't change with d_1. The slider's vibration is still damped out and the slider achieves its steady state quickly. The straight black line in the FH plot is the d_1 line. In both cases the spacing at the rear air bearing center is always above d_1.

Fig. 11 shows the simulation results with the parameter values in Table II except that the friction coefficient μ is changed to 2.0. It is seen that the slider's vibration is again damped out quickly. The increase in friction force has no effect on this 7-nm flying slider.

Fig. 12 shows the simulation results with the parameter values in Table II except that the maximum meniscus force fm is changed to 50 mN. When d_1=0.3 nm, the slider's vibration is damped out quickly and the slider attains a contact steady state. The FH of the steady state is 1.6 nm and the pitch angle is 94.2 μrad. The slider has a lower FH and higher pitch angle than previously due to the large adhesion force of 50 mN. But the slider doesn't bounce continuously on the disk. When $d_1 = d_s$, the numerical calculation doesn't converge even with the time step as small as 10^{-9} s. The spacing at the rear air bearing center is sometimes less than d_s at the beginning of the vertical bouncing. This causes a corresponding sharp change of the rear air bearing stiffness from a positive value to zero. This abrupt change in the rear air bearing stiffness causes the divergence of the

calculation and produces some complex values. These complex values in the simulation result in negative values of system energy, which is shown in Fig. 12 (b).

Fig. 13 shows the simulation results with the parameter values in Table II except that the take-off FH is set to 8 nm, which means that the static flying without considering contact and adhesion is below the take-off FH. In the steady state the slider contacts the disk, which is shown from the non-zero contact force and non-zero system energy. In both cases of d_1=0.3 nm and d_1=d_s, the FH of the steady state is 3.8 nm and the pitch angle is 94.2 μrad.

Fig. 14 shows the simulation results with the parameter values in Table II except that the air bearing damping ratios are changed from 0.01 to 0.002. If d_1=0.3 nm, the slider eventually obtains a steady state. If d_1 is set to be d_s, initially the spacing at the rear air bearing center becomes less than d_1, the system energy becomes negative, but the slider goes to its steady state. The steady states in both cases are the same as the slider's static state. The low air bearing damping ratios only cause a slow decay of the bouncing vibration.

No continuous bouncing vibrations are observed in the simulations with a 7 nm slider. Now we turn to sliders with even lower FHs – a 4 nm FH slider and a 3 nm FH slider. Here d_1 is set to be d_s, the air bearing damping ratios are kept to be 0.002, but the initial FH is varied. The simulation results are listed in Table III. In some cases the numerical solution does not converge, i.e. the numerical scheme does not produce the same result as the time step size is reduced from 10^{-8} s to 10^{-9} s. However, it is seen that none of them show a slider with a continuous bouncing vibration. If the air bearing damping ratios are changed back to the default value 0.01, all of the numerical

calculations converge and the slider achieves a steady state in all of the cases with different initial FH.

As a summary of the above simulations with a simplified air bearing model and a simplified contact and adhesion model, no continuous bouncing vibration of the type shown in Section 3.3 of [1] is obtained. The bouncing vibration can always be damped out and the slider achieves a steady state on a flat disk without micro-waviness. This is in agreement with the results we obtained using the CML air bearing contact model with a smooth disk.

5. Conclusion

Three different nonlinear slider dynamic models are used for the numerical analysis of the bouncing vibration of an air bearing slider in near or partial contact with the disk. In these three slider dynamic models, the air bearing with contact is modeled either using the generalized Reynolds equation modified with the Fukui-Kaneko slip correction and a new second order slip correction for the contact situation, or using nonlinear air bearing springs. The contact and adhesion between the slider and the disk are considered either using an elastic contact model and an improved intermolecular adhesion model, respectively, or using the Ono-Yamane [1] multi-asperity contact and adhesion model. The contact friction is calculated through Coulomb's law. All of the simulation results show that the slider's bouncing vibration is a forced vibration caused by the micro-waviness and roughness. The disk surface micro-waviness and roughness, which move into the head disk interface (HDI) as the disk rotates, excite the bouncing vibration of the partial contact slider. The contact, adhesion and friction between the slider and the disk are not the direct causes of the slider's bouncing vibration, since none of the simulations

predict bouncing in the absence of moving rough disk surface. However, the contact and adhesion affect the bouncing amplitude of a partial contact slider, as analyzed in [12]. So in order to design a partial contact slider with small bouncing, the disk surface, slider-disk contact and adhesion need to be systematically modeled in the simulation process.

Acknowledgement

This research was supported by the Information Storage Industry Consortium (INSIC) and the Computer Mechanics Laboratory (CML) at the University of California at Berkeley.

References

[1] Ono, K., and Yamane, M., 2007, "Improved Analysis of Unstable Bouncing Vibration and Stabilizing Design of Flying Head Slider in Near-Contact Region," *ASME J. Tribol.*, **129**, pp. 65-74

[2] Fukui, S. and Kaneko, R., 1988, ''Analysis of Ultra-Thin Gas Film Lubrication Based on Linearized Boltzmann Equation: First Report-Derivation of a Generalized Lubrication Equation Including Thermal Creep Flow,'' *ASME J. Tribol.*, **110**, pp. 253–262.

[3] Wu, L. and Bogy, D. B., 2003, "New First and Second Order Slip Models for the Compressible Reynolds Equation, " *ASME J. Tribol.*, **125**, pp. 558-561.

[4] Huang, W. and Bogy, D. B., 1998, ''An investigation of a Slider Air Bearing with an Asperity Contact by a Three-Dimensional Direct Simulation Monte Carlo Method,'' *IEEE Trans. Magn.*, **34**(4), pp. 1810–1812.

[5] Chen, D. and Bogy, D. B., 2007, "A Study of Contact Models for Slider-Disk Contact and Impact," CML Research Report, **0702**

[6] Chang, W. R., Etsion, I. and Bogy, D. B., 1987, "An Elastic-plastic Model for the Contact of Rough Surfaces," *ASME J. Tribol.*, **109**, pp. 257-263.

[7] Greenwood, J. A., and Tripp, J. H., 1971, "The Contact of Two Nominally Flat Rough Surfaces," *Proc. Instn. Mech. Engrs.*, **185**, pp.625-633.

[8] Chen, D. and Bogy, D. B., "Intermolecular Force and Surface roughness models for Air Bearing Simulations for Sub-5nm Flying Height Sliders", *Microsystem Technologies*, 2006 [Online]. Available:

http://www.springerlink.com/content/e688147615342264/

[9] Juang, J. Y., Chen, D. and Bogy, D. B., 2006, "Alternate Air Bearing Slider Designs for Areal Density of 1 Tbit/in2", *IEEE Trans. Magn.*, **42**(2), pp. 241-247.

[10] Lee, S-C. and Polycarpou, A. A., 2005, "Microtribodynamics of Pseudo-Contacting Head-Disk Interface Intended for 1 Tbit/in2," *IEEE Trans. Magn.*, **41**(2), pp. 812-818

[11] Ono, K., and Yamane, M., 2007, "Experimental and Theoretical Investigation of Bouncing Vibrations of a Flying Head Slider in the Near-Contact Region," *ASME J. Tribol.*, **129**, pp. 246-255

[12] Chen, D. and Bogy, D. B., 2007, "Dynamics of Partial Contact Head Disk Interface", *IEEE Transactions on Magnetics*, **43**(6), pp. 2220-2222

Table I Parameter values used in the multi-asperity contact and adhesion model for the slider-disk contact (upper asterisks denote the default values used in the simulations)

Maximum meniscus force (f_m)	5.0 mN, 10.0 mN*, 20.0 mN
Take-off FH (d_e)	4.0 nm*, 5.5 nm, 8.0 nm
Friction coefficient (μ)	0.5, 1*, 2

Table II Parameter values used for 2-DOF slider dynamic simulations

slider width (b)	0.3 mm
slider mass (M)	1.59 mg
slider's moment of inertia (J)	2.19×10^{-13} kg•m^2
Distance between the mass center and the contact pad (d_h)	-0.550 nm
Distance between the mass center and the front air bearing center (d_f)	0.250 nm
Distance between the mass center and the rear air bearing center (d_r)	-0.525 nm
Suspension normal stiffness (k)	4.9 N/m
Suspension angular stiffness (k_θ)	1.6×10^{-4} N•m/rad
Suspension normal damping ratio (ζ)	0.002
Suspension angular damping ratio (ζ_θ)	0.002
Static front air bearing stiffness (k_{f0})	5.0×10^{5} N•m
Static rear air bearing stiffness (k_{r0})	1.3×10^{6} N•m
Front air bearing damping ratio (ζ_f)	0.01
Rear air bearing damping ratio (ζ_r)	0.01
Friction coefficient (μ)	1.0
Contact stiffness (k_c)	5.0×10^{6} N•m
Real contact force at the beginning of contact (f_{c0})	5.0 mN
Maximum meniscus force (f_m)	10.0 mN
Touch-down FH (d_s)	3.0 nm
Take-off FH (d_e)	4.0 nm
Static pitch angle (θ_0)	90 μrad
Static FH	7.0 nm
Initial excitation	250 nm FH and 0 μrad pitch angle

Table III simulation results of a 4 nm slider and a 3 nm slider with $\zeta_f = \zeta_r = 0.002$ and $d_1 = d_s$

	Initial FH and pitch angle	Does the numerical calculation converge?	Does the slider achieve a steady state finally?
4 nm slider	100 nm and 0 μrad	Yes	Yes
	50 nm and 0 μrad	Yes	Yes
	10 nm and 0 μrad	No	The FH becomes several microns.
3 nm slider	100 nm and 0 μrad	Yes	Yes
	50 nm and 0 μrad	Yes	Yes
	10 nm and 0 μrad	No	Yes

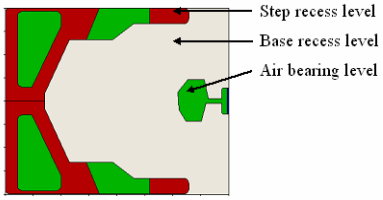

Fig. 1 Air bearing surface design of a micro-trailing pad slider

Case I

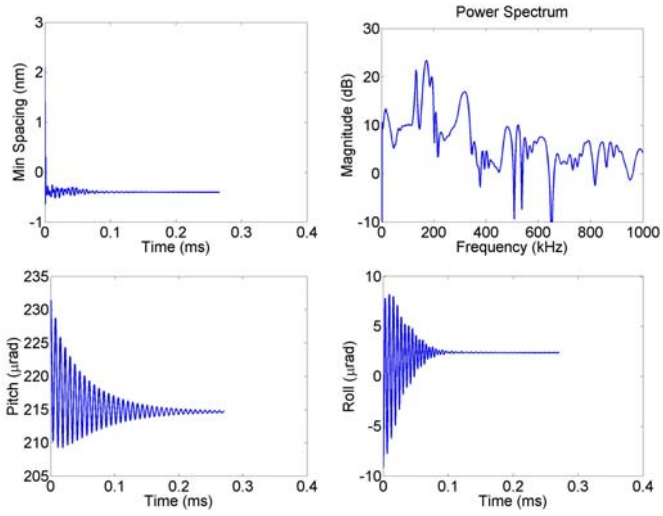

Case II

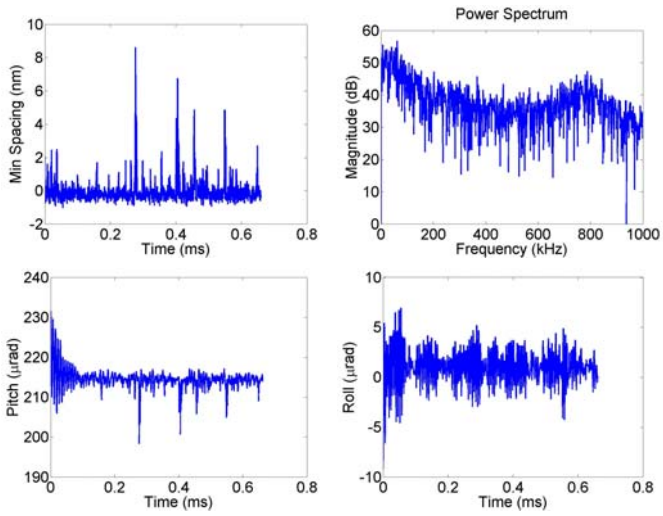

Case III

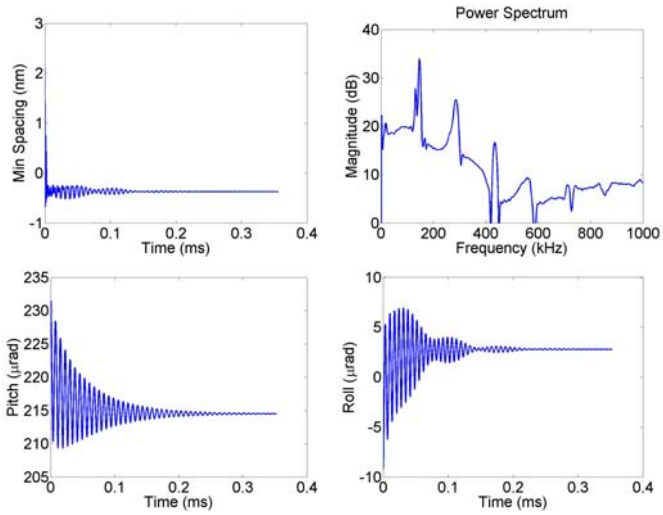

Fig. 2 Time histories of the minimum spacing, the pitch, the roll and the power spectra of the minimum spacing of case I (the micro trailing pad slider on the ideally flat disk surface), case II (the micro trailing pad slider on a rough disk surface with moving roughness within the HDI) and case III (the micro trailing pad slider on a rough disk surface with stationary roughness within the HDI)

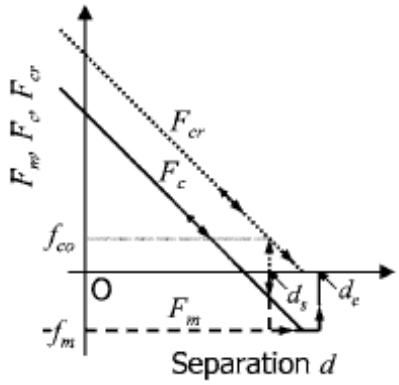

Fig. 3 Simplified characteristic model of real contact force, adhesion force and contact force as functions of separation [1]

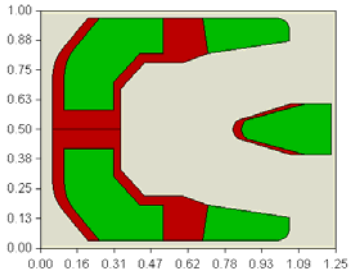

Fig. 4 Air bearing surface design of the CML slider used in the CML 2-DOF slider dynamic simulation

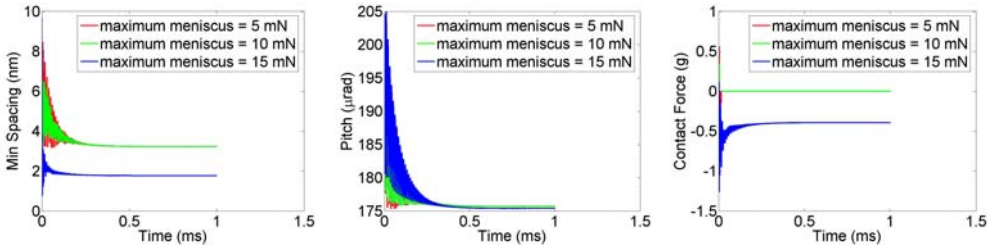

Fig. 5 Time history of the slider dynamics with different maximum meniscus force f_m

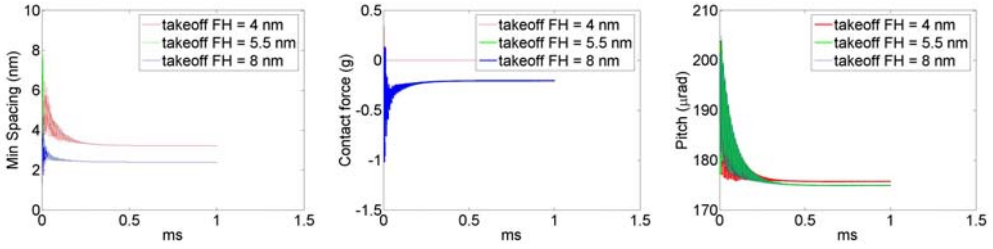

Fig. 6 Time history of the slider dynamics with different take-off FH d_e

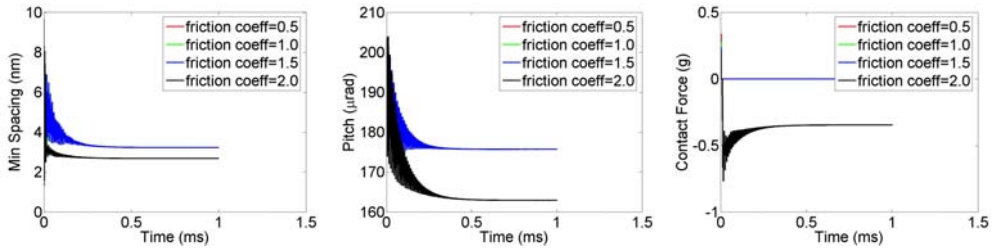

Fig. 7 Time history of the slider dynamics with the different friction coefficient μ

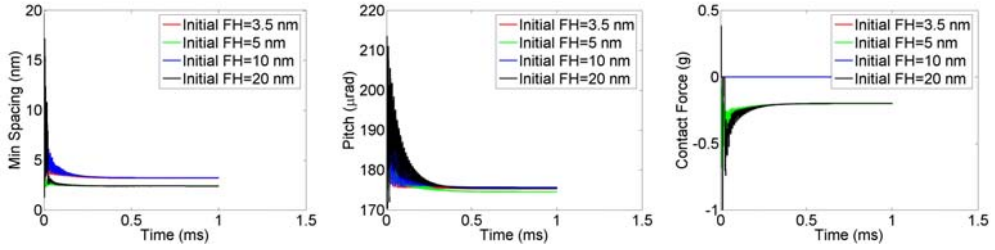

Fig. 8 Time history of the slider dynamics with different initial FH

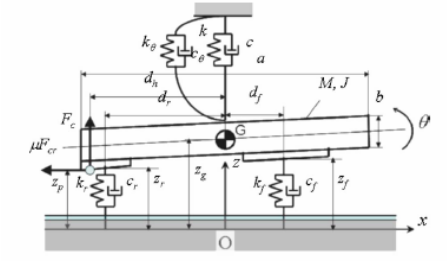

Fig. 9 2-DOF slider model by Ono and Yamane [1]

(a) d_1 = 0.3 nm

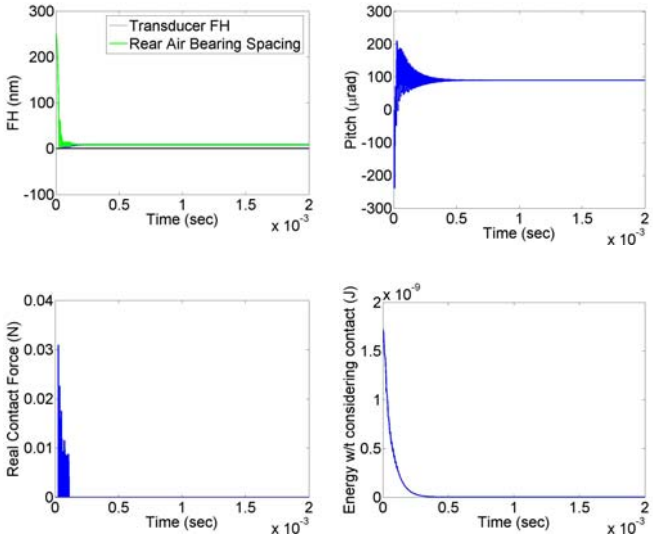

(b) $d_1 = d_s$

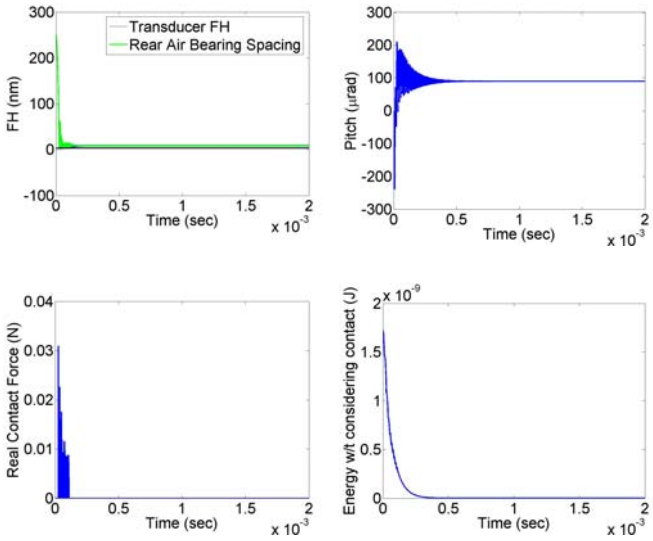

Fig. 10 Time history of the 2-DOF slider model with the parameter values shown in Table II

(a) d_1 =0.3 nm

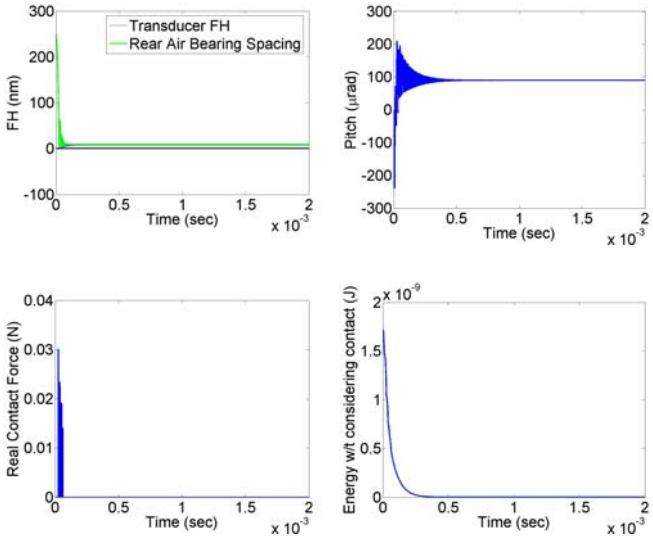

(b) $d_1 = d_s$

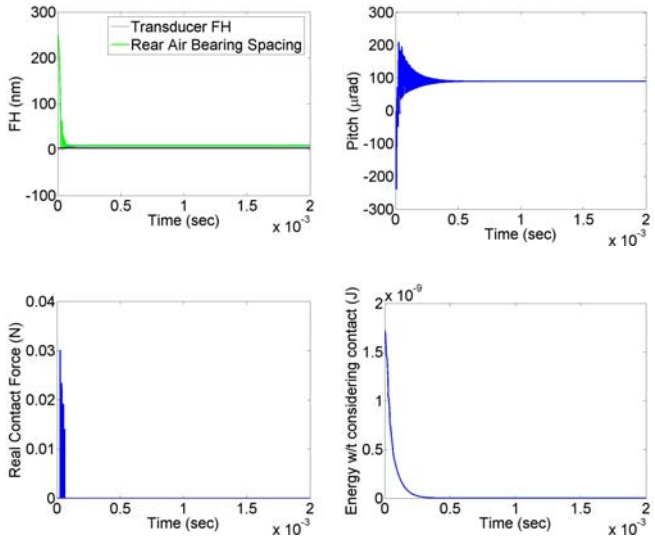

Fig. 11 Time history of the 2-DOF slider model with the parameter values shown in Table II except that $\mu = 2.0$

(a) d_1 = 0.3 nm

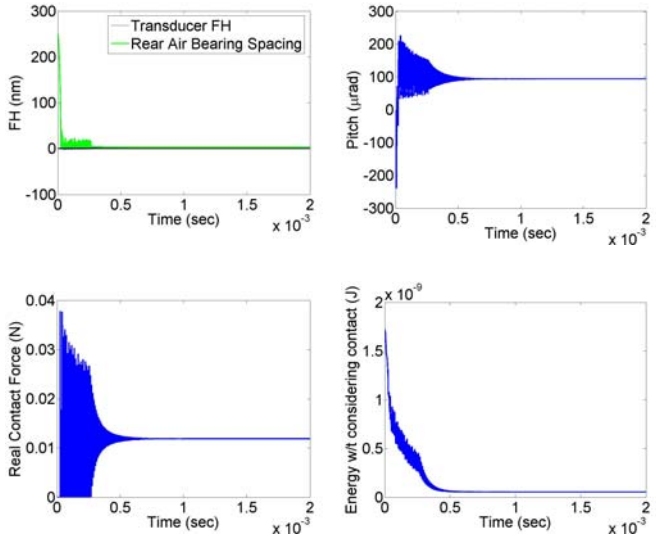

(b) $d_1 = d_s$

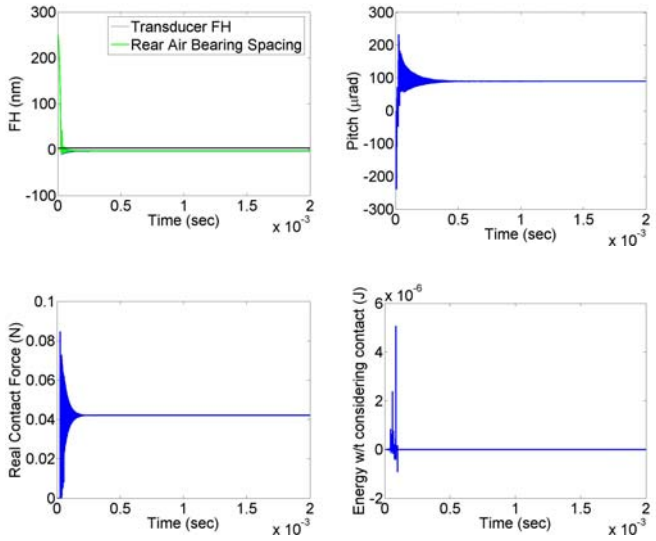

Fig. 12 Time history of the 2-DOF slider model with the parameter values shown in Table II except that f_m = 50 mN.

(a) d_1 =0.3 nm

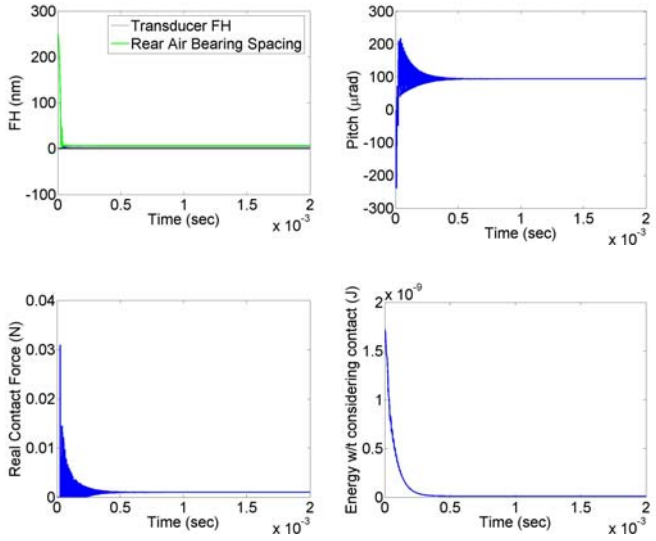

(b) $d_1 = d_s$

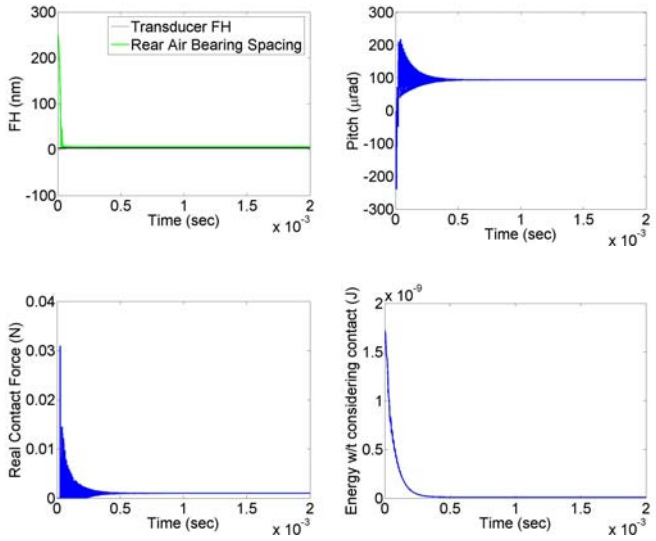

Fig. 13 Time history of the 2-DOF slider model with the parameter values shown in Table II except that d_e = 8 nm

(a) d_1 = 0.3 nm

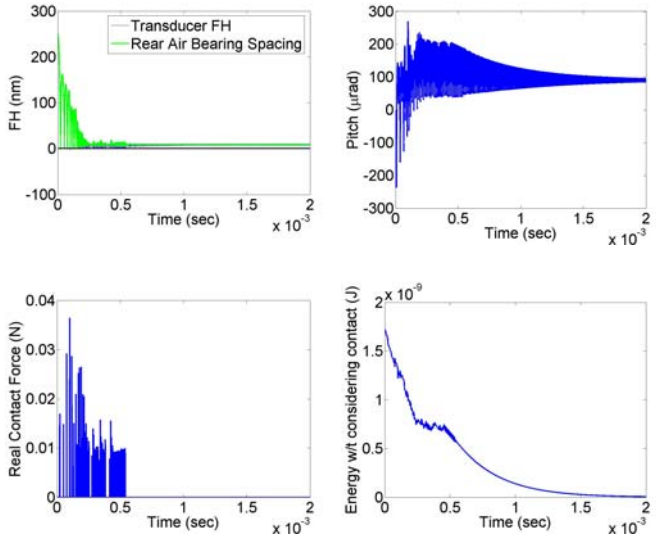

(b) $d_1 = d_s$

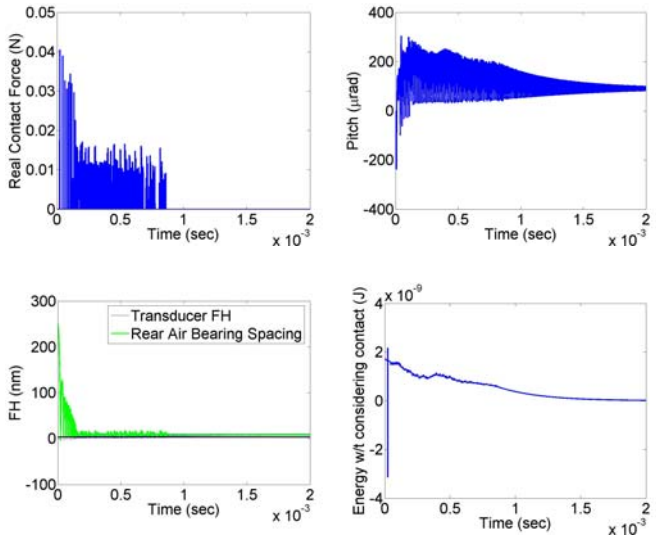

Fig. 14 Time history of the 2-DOF slider model with the parameter values shown in Table II except that $\zeta_f = \zeta_r = 0.002$